GUIDANCE AND CONTROL OF MIR TDL RADIATION VIA FLEXIBLE HOLLOW METALLIC RECTANGULAR PIPES AND FIBERS FOR POSSIBLE LHS AND OTHER OPTICAL SYSTEM COMPACTION AND INTEGRATION

FINAL REPORT

NASA GRANT NO. NAG-1-82

SUBMITTED BY _____
CHUNG YU

ELECTRICAL ENGINEERING DEPARTMENT
NORTH CAROLINA A & T STATE UNIVERSITY
GREENSBORO, NC 27411

GUIDANCE AND CONTROL OF MIR TDL RADIATION VIA FLEXIBLE HOLLOW METALLIC RECTANGULAR PIPES AND FIBERS FOR POSSIBLE LHS AND OTHER OPTICAL SYSTEM COMPACTION AND INTEGRATION

ABSTRACT

Flexible hollow metallic rectangular pipes and infrared fibers are proposed as alternate media for collection, guidance and manipulation of mid-infrared TDL (Tunable Diode Laser) radiation. Certain unique features of such media are found to be useful for control of TDL far field patterns, polarization and possibly intensity fluctuations. Such improvement in dimension compatibility may eventually lead to LHS (Laser Heterodyne Spectroscopy) and optical communication system compaction and integration.

These techniques could further lead to a compact MIR (mid-infrared) laser transceiver (transmitter receiver) package, patterned after near-IR I-O (Integrated Optics) packages in optical communications. Flexible pipes are in many respects superior to fiber interconnections with the possibility of complete closure of source and detection in the same plumbing, provided that the diode source can be

adequately cooled or room temperature sources can be achieved. This cooling may be made possible through the development of microrefrigerators accompanying Josephson Technology. [5]

With current separate source-pipe arrangement, coupling losses are still dominant. Our work is thus concentrated in improvement of the coupling mechanism without resorting to conventional lenses or mirrors. Configurations under consideration are the paraboloid of revolution and the cone tapered guide. Pipe dimensions must also be optimized for maximum flexibility and reasonable linear loss with best mode control.

MIR fibers are not yet practical although extensive work is in progress in research laboratories. Potentials are explored in this work with a view for future MIR optical system integration.

TABLE OF CONTENTS

INTRODUCTION

The mid-infrared region has aroused much interest recently due initially to the availability of the powerful CO_2 laser with stability and tunability. This source has now been further augmented by the lead-salt semiconductor lasers with even greater tunability. The impetus behind the drive into the mid-infrared has been partially powered by lower scattering of such radiation in the atmosphere and thus favored by laser heterodyne spectroscopic systems of atmospheric gases as conducted by NASA.[1] The longer wavelength relaxed fabrication tolerance of guided wave components in devices.

Interest in the mid-infrared (MIR) centered about a wavelength of 10.6 μm has long been fostered due to the unique properties of such radiation. Thus, its propagation through the atmosphere is enhanced by the lower Rayleigh scattering at longer wavelengths, and the wavelength region also covers most of the wavelength signatures of common

polluting gaseous species in the atmosphere. Its invisibility to the naked eye and thus security is, of course, extremely attractive for many security and communication applications. Its practical aspects are further improved by the advent of the highly efficient, high power CO_2 laser with easily accessible frequency stability and multi-line tunability at relatively low costs. Cryogenically operated lead salt diode lasers are now commercially available which add dimension compatibility to fibers and precision near-continuous tunability.

The lead-salt semiconductor diode laser such as $Pb_{1-x}Sn_xTe$, has been extensively used in remote or long-range sensing and point sampling of molecular pollutant gases. This is accomplished by measuring the infrared absorption or emission lines characteristic of a particular pollutant at atmospheric pressure. Point sampling permits gas pressures to be reduced until the Doppler broadened infrared absorption structure is revealed, thereby making possible very high specificity. This method is superior to high quality spectrometers since the latter must be used with reduced resolving power in order to maintain a reasonable signal to noise ratio for relatively low power per unit spectral range available from incoherent sources. The use of a gas laser such as the CO_2 laser, is severely restricted since these lasers cannot be tuned appreciably

from their nominal wavelengths, and the match to pollutant gas absorption lines is seldom ideal.

Semiconductor lasers such as $Pb_{1-x}Sn_xTe$ can be tailored chemically by an adjustment of the composition factor x to emit anywhere in the wavelength range from 6.5 to 32 micrometers, thereby permitting an ideal match to the strong infrared absorption lines of most of the molecular pollutant gases. Individual laser can be tuned by applying pressure, magnetic field or by varying the laser temperature. Thus, such laser can be tuned over a range of 40 reciprocal centimeters quasicontinuously (from one continuous tunable longitudinal mode to another) by changing the diode drive current. This tuning range is sufficient to permit the identification of the spectral signature of a given pollutant even in the presence of other molecular species, and to permit a quantitative determination of its concentration. It has been demonstrated that the linewidth of a 0.24 mW $Pb_{0.88}Sn_{0.12}Te$ diode laser at 10.6 micrometers is 54 KHz (1.8×10^{-6} reciprocal centimeter). By comparison, the narrowest Doppler broadened linewidths of each the heaviest molecular pollutants are tens of MHz at room temperature.

In a typical monitoring application, several $Pb_{1-x}Sn_xTe$ diode lasers would be used, each tailored to emit in a strongly absorbing infrared region of one of the pollutant

gases. This arrangement is necessary due to the limited current tuning range of these lasers, and is desirable because it provides for increased specificity. The small size of these lasers (typically, 0.12 x 0.05 x 0.03 cm) makes it possible for several to be mounted into the same cryogenic Dewar or cold head (at liquid helium temperature for cw operation and liquid nitrogen temperature for pulsed operation).

In actual long path atmospheric transmission study of pollutants, even at atmospheric pressure the collision broadened widths of spectral lines for typical gases are well below the resolution limit of infrared spectrometers now available for field use. In the case of a tunable diode laser, the resolution limit is imposed by the pressure linewidths of the gas itself. If we assume the pressure broadened linewidth of the pollutant gas to be the Doppler width of about 5 Torr, and if we use a Doppler broadened absorption constant per unit pressure of 2 reciprocal centimeters per torr, then the absorption constant α in the transmission factor $\exp(-\alpha L)$ at the center of a strong line at atmospheric pressure is approximately 10^{-5} x concentration in parts per million (α is reciprocal centimeters).

The emitting area of the diode laser in low order transverse mode is 500 by 40 micrometers. If the beam is

expanded 20 times, then the 10 micron laser beam will diverge to an area of 10^5 cm^2 one kilometer from the source. For a collection area of 100 cm^2 at the source and 1 watt pulsed laser power, the collected power without atmospheric attenuation is 1 mW. For an average concentration of 1 ppb over this path, a single change of 1 microwatt is produced, and this change can be measured easily by using synchronous detection techniques. Heterodyne detection of absorption lines with an offset local oscillator should improve the signal to noise ratio because of the narrow emission linewidth of the laser.

The availability of these diode lasers with work on the way towards of the development of room temperature units, and the ongoing intensive efforts in the development of mid-infrared optical fibers have led to the belief of mid infrared optical communication links. The combination of the diode laser and the optical fiber is patterned after visible or near IR optical communication links with a similar extension towards systems compaction and integration. Such may be the trend in the near future.

The use of tunable diode lasers as the local oscillator imposes stringent requirements on their performance with respect to beam profile, polarization, frequency stability and noise properties.

The high refractive indices of these lead chalcogenides and the resulting small critical angles for total internal reflection often cause parasitic nonaxial modes to propagate in these diode lasers fabricated in the conventional manner by cleaving the four sides of the rectangular cavity. In this configuration, these diodes lase in a single-frequency mode with the beam axis in the junction plane, but making a large (15-45 degree) angle with the emitting surface, (Fig. 1) thus giving rise to complex far field patterns. Improvements have been made in fabrication using strip geometry with alleged successful achievement of single-frequency single spatial mode, as reported by the manufacturer.

However, these stripe geometry lasers[2] have consistently been found to emit complex far field patterns which are further complicated by window effects due to the cold head window, in which the laser must be mounted for cryogenic cooling. Qualitatively, the relation between the 10 micron nominal lasing wavelength the 50 micron stripe is of the same order as the lasing wavelength of 1 micron and a stripe 10 micron in the case of gallium arsenide lasers. In the latter, near and far field patterns are reported to differ significantly from the gaussian profile as predicted in wide stripe lasers. Such patterns have been attributed to the finite extent of the stripe. Pure gaussian profiles

correspond to the fundamental mode of an effective waveguide in the junction plane characterized by a strictly parabolic spatial dependence of the complex index of refraction. The non-gaussian patterns are explainable based on deviation of the index of refraction profile from parabolicity. We will follow the same reasoning for the lead salt diode lasers and add that such deviation may be even more severe and difficult to control during fabrication in the case of high values of indices of refraction. This has been the case so far, and the optical feedback introduced by the cold head window is also serious.

Large mirrors and KRS 5 or germanium lenses have hitherto been used to collect, shape and guide such mid-infrared (MIR) radiation. Manipulation of the MIR tunable diode laser (TDL) beam through such optics is time consuming in the laboratory. These optical components also occupy excessive space and their mounting possesses inherent susceptibility to mechanical vibrations, especially in an airborne environment. The shape of the beam guided by the lenses or mirrors is also spatially dependent, i.e., the radiation pattern varies with distance away from the focal point (Fig. 2). The systems also lacks continuous beam steering capability.

In an effort to find an alternate beam guiding medium we first looked to that employed by workers dealing

with near infrared semiconductor lasers and components, where the optical fiber has been gaining acceptance as a transmission medium. [We are projecting and assessing the possibility of extending this available technology to the mid-infrared.]

In the near term, there is, the nonavailability of MIR fibers (they are still in the research stage). As in the case of currently available fibers, substantial losses will be incurred in the source to fiber coupling and fiber to fiber connections. This is essentially the result of dimension incompatibility, and in the case of direct butting, the amount of coupling is proportional to (NA), which can be substantially less than unity. There are also depolarization effects in fibers caused by fiber birefringence and non-circularity. It is assumed that their problems will be alleviated when going to MIR.

As we are approaching the quasi-optical region, some of the well proven microwave techniques may be employed for the control of the quasi-optical beam. The transmission medium, in this case, is the hollow metal piping of rectangular cross section similar to the rectangular waveguide used in microwave plumbing. Radiation from the external source must be collected and coupled into the pipe; or sources can be packaged in such piping if they can operate at room temperature, or microrefrigerators[5] are

available.

Such low-loss piping has been demonstrated to be feasible at 10.6 micron wavelength, while mid-infrared fibers are still in the research stage, but progressing very rapidly. Both media must be studied and compared or combined in possible hybrid systems. Thus, of course, fibers must be used as long haul links, while fibers and piping can be alternate media for the internal packaging of the transceiver unit in optical radar and laser heterodyne schemes. Microwave plumbing is a standard technology with well understood waveguide mode structure and radiation characteristics; mid-infrared optical fiber is still not yet commercially available, and its propagation characteristics are not as rigidly controllable.

Coherent optical fiber transmission systems, in which the amplitude, frequency and phase of the coherent carrier wave such as the laser beam are used to modulate and demodulate high capacity information efficiently, have several preferable features as compared to conventional PCM-IM direct detection systems. They will have signal receiving level limited only by the signal shot noise provided the local oscillator has sufficient optical power at the receiver. Receiver signal level at a prescribed error rate is markedly improved. Spurious optical spectrum outside the signal band can be filtered by means of highly

selective optical heterodyne or homodyne detection. The frequency filtering property is effective in improving the noise performance of optical amplifier-repeater systems and in space communication systems using carrier wavelength longer than 3 microns, in which the main noise source is incoherent broadband spontaneous emission and background light. Optical heterodyne detection converts the carrier frequency from about 200 THz in the optical region to several GHz in the RF region. Advanced signal processing techniques such as FSK or PSK signal modulation and demodulation, frequency multiplexing and demultiplexing, and local oscillator frequency stabilization are well established in the microwave and mm wave technology.

Optical heterodyne or homodyne detection is sensitive to the mismatch in wavefront, frequency, phase and polarization states between the signal and local oscillator waves. In a way, this mode selective character is advantageous for the suppression of background light noise and also opens the possibility of spatial mode multiplexing systems, while stringent requirements are imposed on spatial alignment and frequency stability.

Hollow metal piping not only possesses the capability to define the wavefront and polarization of the transmitter and local oscillator, but also the received signal, if the latter is collected and channeled to the

mixer through the same piping. The beat, which is in the microwave region can be tapped from the mixer with good impedance matching through conventional microwave waveguides and waveguide transitions and tuning stubs. Thus, there is excellent dimension compatibility in the sense of the transceiver package.

At this stage in a parallel vein, polarization preserving optical fibers have been successfully fabricated in the near IR in the elliptical form. In the concept of the transceiver package, there is an advantage of reduction in size and weight. However, the coupling of radiation from external sources into the fiber, which then has to exit and be incident on the external mixer, probably located in a microwave waveguide for propagation of the GHz beat frequency, imply dimensional incompatibility.

There is at present at issue the interface problem between the rapidly advancing technology of optical links and the interconnection to existing or planned RF or microwave links. The problem lies in the significant design criteria of these two systems. Thus, optical systems are characterized by low power levels, high data rates, wide bandwidths, and tend to favor pulsed operation, while RF links are generally high powered, relatively low data rates, constrained bandwidths, and almost always use cw operation. This means that a direct interconnection can often produce a

communication bottleneck and a combined system degradation, even though both systems may have been separately optimized. Thus, the interface problem lies in interconnection of optical-RF or RF-optical systems. Heterodyning may thus prove to be an excellent means of natural interfacing of RF using the beat signal.

The design of the transceiver package is thus extremely important in optical communication systems using optical heterodyning or coherent detection. In this instance, metallic piping and fiber each has its own strong and weak points, the former in weight and the latter in lack of controllability and nonavailability at this time. Thus, both media must be investigated.

HOLLOW PIPE WAVEGUIDES (See Appendix A)

Patterned after microwave, hollow metal pipes can be used as low-loss waveguides for MIR radiation. One hundred percent transmission[1] has been observed at 10.6 μm through a 13" long waveguide fabricated from unanodized "one side bright" aluminum along the broadside and brass shim stock (Fig. 3) as the narrow walls giving a .5 mm x 7 mm cross-section. This belt-like construction provides the necessary flexibility for bending and twisting, and thus ease of manipulation of the guided beam in optical systems.

Unanodized aluminum is favorable due to its high infrared reflectivity as well as flexibility. This material does have finite conductivity which means that there is some absorption of power when radiation is reflected off its optically smooth surface. This is why unanodized aluminum has a complex index of refraction, which is dependent upon wavelength of incident radiation. The imaginary part of the refractive index describes reflection while the real term determines absorption. Metals used in the infrared have refractive indices whose absolute values are much greater than unity.

At such a long (10.6 μm) wavelength, light basically grazes the walls of a waveguide without the scattering that visible light would incur. Low mode-order increases are thereby possible for light with less tendency of higher order modes being forced into transmission. High order modes are discouraged by the conductivity of the aluminum. High order modes in the transmitted radiation means equally high order current distribution patterns in the aluminum. These modes would not be possible in a dielectric, and attenuate rapidly due to power lost as heat. This favoring of lower modes is of unquestionable value to the Tunable Diode Laser.

The TDL lases at ~10.6 μm from a point source and is notorious for complex far-field patterns (Fig. 4). These

complex patterns can be a problem in optical systems, and a transmission medium that limits propagational modes to lower orders simplifies the pattern. Simpler patterns are favored because they make optical devices such as detectors more reliable as accurate component in an optical system.

There are two basic types of polarization, TE (transverse electric field) and TM (transverse magnetic field), for plane waves in this waveguide (Fig. 5). The polarization is always with respect to a plane parallel to the aluminum walls of the guide. This is due to the constant rectangular cross-section of the waveguide which keeps the boundary conditions of the wave consistent down the length of the pipe. Therefore, the plane and type of polarization of an input wave is not changed in the output wave. This feature is also favorable in optical systems since some devices are polarization sensitive.

Ray optics is very useful in analyzing some optical systems. In order to make the ray optics approximation, the loss in the walls (i.e. current flow) must be accounted for. Basically, there is an ohmic loss associated with a reflection. Multiplying the loss from one reflection by the number of reflections a ray makes down the length of a waveguide and the result is the total loss from the waveguide. Ray optics explains why the loss in the brass walls is neglected and we can assume plane wave

propagation. There are so few bounces off the sidewalls in comparison to the aluminum walls that the loss can be ignored in comparison.

In analyzing the reflection loss for a ray off the aluminum walls, it works out that the single reflection loss is angle dependent. The larger the grazing angle, the greater the power lost. Higher order mode rays reflect at steeper angles and they reflect more times per unit length. Therefore, lower order modes suffer lower loss for two reasons; less loss per reflection and smaller number of reflections.

Bending a waveguide is useful in manipulating a beam in an optical system. Ray optics illustrates the effect of a bend on the propagation of MLR radiation. Basically, the radius of curvature of a bend must be much greater than the spacing between the two aluminum walls which are being bent along an axis perpendicular to the direction of propagation. Too severe a bend would prohibit transmission altogether. When the bending is of an acceptable degree, both aluminum walls are bent with approximately the same radius of curvature and the cross section is kept constant. This assures that the polarization will be preserved.

Sufficient bending creates a mode known as the "whispering gallery mode" in which all reflection is off the

outside wall (Fig. 6). There is no interaction with the inner wall in the wig-mode. Propagation is assumed to be in the direction perpendicular to the radius of curvature rather than in a straight line, but the loss is formulated by summing up single-reflection losses just as in the straight waveguide case.

Just as single reflection losses are dependent upon angle of reflection in the straight guide case so are they in the bent guide case. This become an inverse dependence on radius of curvature for bent waveguides since the smaller the radius of curvature the greater the angle of reflection. Total loss over a length of a bent waveguide is independent of wallspacing. This is due to the fact that there is only interaction with one wall. The order of the mode before going into a bend has no bearing on the loss in the bend since the light is forced into a wig-mode.

There are distinct orders of wig-modes, but basically a higher order mode will have the same loss as a lower order mode since although there are more reflections for the higher order case, the angle of reflection is less and they exactly balance each other. Basically, the loss encountered through a bent waveguide is the same as what would be encountered with a single reflection mirror of the same aluminum. A mirror may be the best method of bending the beam path in some instances.

Twisting a waveguide presents a different problem from that of a bent guide (Fig. 7). Twisting guide is done by rotating one section with respect to another about its center axis along the direction propagation. The modes in a twisted waveguide are the same as those in a straight waveguide. The plane of polarization is obviously twisted as is the guide, but the modes are consistent along the twisted plane.

Ray optics illustrates why polarization is preserved for the twisted case. Reflection off a wall in a twisted section of a waveguide tilts the polarization of a ray, but that tilt is canceled out by the effect of reflection off the opposite wall. This "canceling out" guarantees that polarization is preserved from input to output with respect to the transverse plane.

The distance between the waveguide wall determines the angle at which a ray is reflected in a twisted section of waveguide. The greater distance between the walls, the steeper the angle of reflection. Steeper angles of reflection mean greater loss due to absorption. Therefore twist loss is proportional to waveguide height. Experiments were done to verify this dependence as well as other predictions of waveguide performance; the experimental setup is shown in Figure 8.

The TDL is contained inside the closed cycle cooler and the mirrors allow using either the TDL or the CO_2 laser as input for any of the pipe-detector set-ups. The detectors are on translational stages so that beam profiles may be measured through the lock-in amp on the X-Y recorder. The monochromator is set up to observe spectral composition before and after the hollow pipe waveguide.

The TDL current drive was internally chopped so that the radiation could be fed to the lock in amplifier with the output traced out on a X-Y recorder. The detector with a 1 mm x 1 mm-aperture was mounted on a motor driven translational stage with a 2 inch travel. Figure 9 shows a complete TDL radiation pattern beyond the cold head window approximately 1 inch from the diode emitting surface. The observed spatial profile exhibits a complex structure comprising of two main lobes and some minor lobes due possibly to window effects.

To investigate the beamshaping capability of the pipe, its radiation was scanned progressively further away from the exit and of the pipe. As Figure 10 shows, the beam radiated from the pipe held its width but with decreasing intensity, indicating a highly directional beam. The last figure illustrates what the radiation pattern would appear like without the pipe. The advantage of the pipe over lens focusing is illustrated by Figure 2. Although the radiation

pattern is well behaved in the focal plane, it degrades very rapidly going away from that plane. This makes alignment accuracy much more critical in the lens set-up.

The TDL lasing spectrum was analyzed before and after transmission through the pipe (Figure. 11), and no significant difference in the spectral composition was observed. Lower transmission was also observed without significant variation in the radiation pattern when the pipe was slightly bent. Figure 12 illustrates that losses in the pipe are independent of waveguide height by showing the results of an experiment done with two pipes of different heights being bent and having the output power measured. Both of the pipes incurred the same losses from bending. Twisted pipes, on the other hand, demonstrated a height dependence for loss as expected and as illustrated in Figure 13.

This promising infrared guiding medium should certainly be further studied for the improvement of input coupling efficiency. Cylindrical lenses have been used extensively as coupling devices, focusing either a CO_2 laser or TDL beam down to a line segment into the waveguide. In terms of efficiency and durability (since lenses can be permanently attached to guide), the cylindrical lens fared well. But in the overall integration "game-plan" it is a step backwards. Ideally, an integrated optical system would

not contain discrete optical components such as lenses or mirrors.

Tapering the waveguide's input end is done sometimes in conjunction with using an input lens. A straight taper (Figure 14) complements the cylindrical lens quite well, since the beam is being focused a minimum of reflection off the tapered section is required. In considering curvatures for tapered ends, of all possibilities a parabolic curvature seems to fill the most needs of an isolated source such as a TDL.

The advantage of a parabolically tapered end is that any ray projected parallel to the parabola's axis will be focused to a point. If the axis of the parabola is aligned with the waveguide's long dimension axis then radiation should be effectively coupled into the guide. This coupling scheme is useful when considering that rays entering the tapered end are very nearly parallel. If one then considers the whispering gallery mode, then the idea of light "hugging" the tapered wall in whispering gallery fashion is certainly applicable.

In an effort to couple even more light into the waveguide, a system known as the compound parabolic concentrator (CPC) has been developed. Basically, the CPC consists of two parabolically tapered sections with

different focus.

The ultimate coupling devices may be the grating as illustrated in Figure 15. This coupling scheme is very compatible with a substrate environment and it is conceivable that a similar waveguide can be fabricated by methods of planar technology and similarly in the place of brass shim stock side-walls, dielectric walls can be etched instead. Grazing incidence reflection rather than metallic reflection confines the light which would allow for a narrower waveguide, since no currents are induced in dielectric.

OPTICAL FIBERS

The surging development of optical fibers is the biggest reason why optical systems are being integrated. Optical fibers finally provided a reliable long-range transmission medium thatis flexible,efficient but not yet totally understood. Optical fiber technology now is fast growing and integrated optics must grow fast to keep pace.

Mid-infrared (MIR) optical fibers are quite a different story. Up to this point in time, there are no cladded MIR fibers available. Air serves as the cladding (Fig. 16a). There are also no single mode MIR fibers, since they would ha to be very thin. Also, hygroscopicity (dissolving in

water) is a problem with some materials used in MIR optical fibers.

The limiting factor in most optical fiber transmission is Rayleigh scattering. Rayleigh scattering is intrinsic to the most transparent of materials and it sets the minimum amount of attenuation possible at a particular wavelength when light is transmitted through a fiber. Rayleigh scattering is proportional to λ^{-4}, therefore theoretically the longer the wavelength of light the less loss in transmission. Purity of materials is very important since impurities tend to act as absorption centers. The lowest loss reported so far in MIR fibers is .4 dB/m. This fiber was made of KRS-5 (thallium bromoiodide) which also performed best for transmission of high power density at 12 cw/cm^2, [6] before damage was incurred.

The reduction of impurities is the key to better MIR fiber performance at this point in their development. Technical improvements in the fiber fabrication process have led to less impurities and defects in these fibers. The consistency of circularity is the key to having fibers that preserve polarization from input to output.

Nuclear radiation is a problem to all electronic

systems. Fiber optic systems in the visible range have demonstrated no better performance in nuclear radiation than wired systems[7]. Basically, radiation is capable of darkening the fiber material which causes light to be absorbed, and thus degradation of system performance.

The same is not true of MIR fibers. Since the wavelength is longer than in the visible range, the darkened fiber material will not absorb light as extensively. Infrared light is invisible, so only defects caused by nuclear radiation could possibly deter transmission, since the color of the material does not matter.

Fibers demonstrate an advantage over waveguides in that reasonable bending and twisting do not affect transmission. This, along with their potentially lower loss and less expense per length, gives fibers the edge in terms of long distance optical transmission. But fibers and hollow pipe waveguides both would benefit from further development in coupling schemes.

Direct butting of a fiber to a laser source is the most desirable method. Butting would reduce window effects to a minimum and maximize coupling efficiency. In the case of the TDL, some new technology needs to be developed before this can be achieved, but when the technology is ready perhaps fibers will be ready.

COMPOUND PARABOLIC COUPLING OF TDL RADIATION INTO A HOLLOW PIPE WAVEGUIDE

For the purpose of coupling light into a hollow pipe waveguide, the CPC[8] is of unquestionable value. It's design is that of a paraboloid extended into 3-D by revolving it above an axis that intercepts its own (Fig. 18) and taking the interception of the paraboloid of revolution with a single plane and extending it along a plane perpendicular to that of the 2-D case . The angle at which the axes intercept after revolution becomes the angle at which a ray of light would be able to enter the CPC's entry aperture and exits through the exit aperture (using a geometrical optics approach). The concentration ratio is the ratio of entry aperture's height (a) to that of the exit aperture (a'). Once the maximum collecting angle and height of either aperture has been decided, all other design parameters (concentration ratio, length, focal distance of parabola) are set. Any ray entering the entry aperture of the CPC at an angle (w.r.t. axis of CPC) less than or equal to θ_i (maximum collection angle, m.c.a.) will aperture.

The edge-ray principle states that all rays entering the entry aperture at an angle θ_i should emerge from the rim of the exit aperture. Therefore, the angle at which a ray, that barely eludes the wall of the exit

aperture, enters, is the m.c.a. CPC's are constructed using the edge-ray principle (Fig. 19). It is a matter of simple coordinate geometry (Appendix B) to show that the focal length of the parabola is

$$f = \frac{a'}{2} (1 + \sin\theta_i) \tag{1}$$

the overall length is

$$h = \frac{a'}{2} (1 + \sin\theta_i) \cos\theta_i / \sin^2\theta_i \tag{2}$$

and the height of the entry aperture is

$$a = a'/\sin\theta_i \ . \tag{3a}$$

We see from this that the maximum theoretical concentration ratio

$$a/a' = 1/\sin\theta_i \tag{3b}$$

provided all of the rays inside the angle θ_i actually emerge from the exit aperture. This is not exactly the case, due to the fact that rays that strike the edges of the exit aperture will scatter and some will not exit.

If the height of a CPC's exit aperture is made to be the height of cross section of the hollow pipe waveguide and it is tapered into the pipe's cross section with axis

parallel to the pipe's walls, then the fundamental mode of the waveguide would be excited favorably by MIR light coupled from the entry aperture. Two applications can utilize the CPC's properties. First is the collection of radiation from distant sources, with the possibility of application to laser Heterodyne spectroscopy. Radiation from distant sources comes in essentially as plane waves. The rays of plane waves are parallel, therefore if they are aligned with the axis of the CPC (simply by aiming it), then θ_i need not be very large at all. Since the concentration ratio is inversely proportional to $\sin\theta_i$, a small θ_i affords a large concentration ratio and thereby a large area from which radiation can be collected. Second is the coupling of MIR radiation from a TDL source. The case of the TDL is not as simple as that of distant sources due to the high divergence of the TDL. This application will be covered more extensively.

An efficient coupling scheme for the TDL must take into account the fact that the diode is housed in a cold head and the laser is emitted through a window in the cold head. This fact restricts access to the laser source and stipulates that the entry aperture to the CPC be as large as the window and accepts rays at the angles of departure from the window. Assuming that the window does not change the angle of the rays considerably, it would be impossible to meet

the requirements of a typical TDL (Fig. 20) with a CPC. This fact is due to the angular dependence of the concentration ratio and the requirement that the diameter of the entry aperture be at least that of the cold head window. The cold head window is designed to transmit all of the diode's light while separating the environment of the diode from that of the outside. The same compulsory job could be accomplished by a lens with the extra feature of collimation. There is motivation (as previously stated) to eliminate conventional optical components, but as long as a window is necessary it may as well serve as many uses as possible. A half convex spherical lens with a focal length equal to the distance from the source to the window would serve as an effective collimator if the axis of the lens is aligned with the junction (Fig. 21).

With a collimating lens, rays traveling into the entry aperture would be very nearly parallel to the CPC plane and θ_i need not be very large. Therefore, the concentration ratio can be high. The exit aperture height for hollow pipe waveguide use, should be approximately .5 mm. The entry aperture is required to be on the order of 25 mm in order to be compatible with the cold head window of the TDL.

The concentration ratio associated with two such apertures is approximately 50. Using aforementioned

formula, the acceptance angle may be calculated as

$$\theta_i = \sin^{-1}(a'/a) \ . \qquad (3c)$$

Therefore, θ_i would equal approximately 1.13° or that only nearly parallel rays would pass through such a component. It is feasible that such a component could be useful even with such a small θ_i. Feasibility is severely tested when considering the length of this device which is formulated from (2) as > 1.3 m.

Even considering the polarization maintenance capabilities of such a component may not justify a coupling structure of such length. In designing another coupler two facts must be considered (1) that any coupler of rectangular cross section will preserve polarization and (2) most of the energy leaving the cold head window is concentrated near the center. These facts imply that another curve, besides a parabola may be useful in the final design of an appropriate coupler. The simplest of curves is a straight line and a straight taper can be designed with a maximum acceptance angle and aperture height compatible to a CPC section.

The following specifications are not necessarily optimal, but illustrate one method of utilizing some length (in this case 200 mm) as a coupler length. The idea is to use a straight tapered section going into a truncated CPC.

The small end of a CPC will transmit rays directly into the pipe, but will be truncated (cut away from its larger end at some distance $L-L_T$). The greatest concentration of rays (at the center of the window) will interact only with the truncated CPC section if the axis of the window lens is also the center line of the truncated CPC's plane of symmetry. The longer the truncated section and the smaller its θ_i, the larger its entry aperture height will be. This entry aperture height controls the amount of light that is virtually all coupled into the hollow pipe. The straight tapered section will undoubtedly have a greater θ_i (Fig. 22) than the final section and greater loss but aptly serves as an interface between the window and the truncated section.

The actual radiation pattern of the particular TDL diode needs to be taken into account to design the optical coupling section. For the sake of simplicity (which is why a straight tapered section was initially incorporated), 150 mm is designated as the length of the truncated CPC leaving 50 mm for the straight taper, θ_i for the truncated section will be 1.75°, which is approximately the maximum angle that single mode light would graze the hollow pipe waveguide. This is calculated as follows:

$$kx\ (max) = \frac{\Pi}{h} \tag{4}$$

$$k\ min\ \sin(0\ max) = \Pi/h$$

$$\frac{2\Pi}{\lambda\ (max)}\ \sin(0\ max) = \frac{\Pi}{h}$$

$$\frac{2\Pi}{.03\ min}\ [\sin(0\ max)] = \frac{\Pi}{.5\ mm}$$

$$\sin(0\ max) = .03$$

$$\sin(0\ max) \leq 1.75^{o}$$

Where kx is the transverse component of the propagation vector perpendicular to the top and bottom walls, h is the height of the waveguide and λ(max) is the longest wavelength radiated from the TDL ($\simeq$ 30 μm). As shown in Figure 23 single mode operation requires that the above boundary condition be met.

According to the following formulas

$$h_T = \frac{f\ \cos(\phi_T - \theta_i)}{\sin^2(\frac{\phi_T}{2})} \tag{5}$$

$$a_T = \frac{2f\ \sin(\phi_T - \theta_i)}{\sin^2\frac{\phi_T}{2}} - a' \tag{6}$$

where h_T and a_T are the length and entry aperture height after truncation and ϕ_T is the angle in Figure 22, where the entry aperture height is 15.5 mm. Using that as the exit aperture

height of the straight tapered section, a maximum acceptance angle of 22.3^{o} is calculated by using the edge ray principle and trigonometry, figuring that the entry aperture to the straight tapered section will be a 1 inch square.

Not mentioned before is the other dimension of the coupling section which must shrink from 1 inch at the front of the straight tapered section to 6 mm at the beginning of the pipe. Depending on the actual radiation pattern of the diode, little light should interact with these sidewalls. Therefore, a straight taper will suffice as in Figure 22.

Experiments need to be done on this type of section before optimization in design is possible.

APPENDIX A

Flexible infrared-transmission metal waveguides[4]

The waveguides studied were rectangular in shape and fabricated by clamping together commercially available "bright" aluminum sheet separated by brass shim stock whose sides were carefully machined sharp and flat. The structure is shown in the inset of Figure A2. The optical losses were determined at 10.6 μm by comparing the transmission of CO_2 laser light in a 10-cm guide to that in 1-m guide. The polarization was chosen parallel to the long dimension of the guide so as to propagate TE modes. The waveguides were excited primarily in the lowest-order mode by that part of a CO_2 laser beam, 1 cm in diameter, which entered the guide. The near-field pattern at the exit of the guide was a single bright line, and the far-field divergence angle in the rapidly spreading direction was 1°, consistent with that expected for a single mode.

The measured transmission of a 1-m planar straight waveguide is shown in Figure A1. The theoretical expression for the exponential power loss coefficient for the TE_{10} mode is a planar hollow metal waveguide of height a is

$$\alpha_{TE} = (\lambda^2/a^3)\ \mathrm{Re}(1/\nu) \qquad (A1)$$

where λ is the wavelength of the light and ν is the complex refractive index of the metal. For "ideal" aluminum, freshly evaporated on an optically flat surface, $\nu = 20 - i59$. The theoretical transmission for a waveguide having such surfaces is shown as a function of a in Figure A1 and is labeled "ideal".

In our experiments we used commercially available aluminum called "one side bright". Measurements of waveguide transmission using this material are shown as the experimental points in Figure A1. In order to compare the experimental waveguide transmission with the theory of Eq. (A1), it is necessary to know the reflectivity of the commercial surface. Its reflectivity at 80^0 from the normal was measured and compared with the "ideal" reflectivity. The measured reflectivity was 94%, indicating a 6% single reflection loss. This is 16 times larger than the "ideal" case, in which the reflectivity should be 99.63%. This indicates that the "commercial" waveguide loss coefficient will be 16 times larger than the "ideal case". The expected waveguide transmission using Eq. (A1) and the measured commercial surface reflectivity is plotted in Figure A1 and labeled "commercial". The experimental measurements of waveguide transmission agree well with the theoretical transmission.

From the agreement between measured waveguide transmission and the theoretical values calculated from measured reflectivities, we can see that surface smoothness and waveguide fabrication techniques are not critical factors in determining waveguide loss. This is in contrast to visible wavelengths at which the shorter wavelengths require smoother walls. Better waveguide transmission is possible using surfaces which have a higher large-angle reflectivity. We expect to optimize waveguide transmission by optimizing single-surface reflectivity. In Figure A1 we have shown the "ideal" copper waveguide transmission, which is probably the best material available for use at 10.6 μm. We believe this is the order of waveguide transmission which can be achieved in the future.

The sidewalls, which acted as spacers for the planar waveguides, were brought closer together to form a rectangular waveguide of width b and height a. In this case the planar TE mode is perceived by the sidewalls as a TM mode. These walls add the following contribution to the exponential loss coefficient :

$$\alpha_{TM} = (\lambda^2/b^3)\ \mathrm{Re}(\nu) \qquad (A2)$$

In Figure A2 we show the transmission of a 1-m rectangular guide as a function of the width of the guide, normalized to the planar guide transmission. The theoretical curve is for

an estimated real part of the refractive index for brass of 22. We do not know the exact composition of the brass we used, or the exact value of the complex refractive index, but this is a best estimate in comparison to known metals. The experimental measurements shown in Figure A2 lie near the theory. This indicates that the carefully machined brass sidewall surfaces have sufficiently high reflectivity at grazing incidence angles to make low-loss waveguides.

These rectangular metal waveguides are of interest at 10.6 μm because of the possibility of developing fully flexible waveguides. The ability to transmit large amounts of power in the infrared in a fashion analogous to the transmission of visible light through fiber optics will prove useful for cutting, welding, and heat-treating applications. There are preliminary measurements of bending loss to demonstrate the potential of these waveguides. One-meter long planar guides were bent in a direction perpendicular to the plane of the waveguide, as shown in the inset in Figure A3. We measured the transmission of these waveguides as a function of the bending radius and normalized the transmission to that of a straight guide. The guides were curved at the measured bending radius for a length which was roughly 50 cm, and were straight at their entrance and exit. Measurements of the transmission of these bent guides relative to the

straight 1-m guides are shown in Figure A3 for two values of waveguide height. Data from these measurements fit an exponential loss coefficient which is inversely proportional to the square of the bending radius R, and are labeled "commercial" in FigureA3.

The exact theory for a bent rectangular waveguide has not been worked out; however, we expect the contribution to the exponential loss coefficient from bending to have the form

$$\alpha_R = \alpha_s \eta_{pq} a^6/\lambda^4 R^2 , \qquad (A3)$$

where α_s is the straight guide loss and η_{pq} is a geometrical factor. η_{pq} has been calculated for bent cylindrical guides and has only been estimated for bent rectangular guides. The factor η_{pq} depends on the mode and decreases rapidly as the mode order increases. According to Eq. (A3), the bending loss should have a strong dependence on the height of the waveguide. Experimental results do not bear this out. We do not understand the discrepancy between the expected theory and the measurements at the present time. There are, however, several possible explanations related to the rudimentary nature of our present theories and experiments. Examination of the output mode profile, viewed on an infrared-sensitive phosphor, shows that the shape changes considerably for large bends. This may

indicate that we are in a regime of bending for which present theories are inadequate. In addition, we may be observing conversion to the higher-order modes preferred in bent waveguides [see Eq. (A3)]. In these experiments the bending did not occur uniformly throughout the guide and the transitions from straight to bent guide may affect the results. Finally, these preliminary bending measurements employed primitive waveguide fabrication techniques. The aluminum strips were held together with a number of separate clamps to achieve flexibility. This is in contrast to the straight waveguide which was clamped uniformly between the two flat rigid plates.

The straight transmission of each waveguide was considerably smaller than the straight guide transmission results shown in Figure A1. This may have been caused by the use of many independent clamps, which caused local thickness variations in the straight guide.

APPENDIX B

The Geometry of the Basic Compound Parabolic Concentrator[8]

Is is probably simplest to obtain the basic properties of the CPC from the equation of the parabola in polar coordinates. Figure B.1 shows the coordinate system. The focal length f is the distance AF from the vertex to the focus. The equation of the parabola is, then,

$$r = 2f/(1 - \cos\phi) = f/(\sin^2 \tfrac{1}{2}\phi) \qquad (B1)$$

this result is given in elementary texts on coordinate geometry and it may be verified by transforming to polars the more familiar cartesian form, $z = y^2/4f$ with axes as indicated in the figure.

We apply this to the design of the CPC as in Figure B.2. We first draw the entrance and exit apertures PP' and QQ' with the desired ratio in aperture between them, and we choose the distance between them so that an extreme ray PQ' (or P'Q) makes the maximum collecting angle θ_i with the concentrator axis. The profile of the CPC between P' and Q' is a parabola with axis parallel to PQ' and with focus at Q, and this parabola can be expressed in terms of

the polar coordinates (r,ϕ) as on the diagram.

For the exit aperture we have, using Eq.(B1)

$$QQ' = 2f/[1 - \cos(\pi/2 + \theta_i)]$$

so that is $2Q' = 2a'$, in our usual notation

$$f = a'(1 + \sin\theta_i) \tag{B2}$$

Next we find

$$QP' = 2f/(1 - \cos 2\theta_i)$$

or

$$QP' = a'(1 + \sin\theta_i)/\sin^2\theta_i \tag{B3}$$

Thus

$$a + a' = QP' \sin\theta_i = a'(1 + \sin\theta_i)/\sin\theta_i$$

so that $a = a'/\sin\theta_i$, as required. Finally, for the length of the concentrator

$$L = QP' \cos\theta_i = a'(1 + \sin\theta_i)\cot\theta_i/\sin\theta_i = (a + a')\cot\theta_i \tag{B4}$$

This, of course, is again as required by the way we set up the design of the CPC.

It is obvious from the geometry of the initial requirements for the CPC that the profile at P and P' should have its tangent parallel to the axis. This also can be verified from the above formulation. For the tangent of the angle between the curve and the radius vector is, in polars,

$$\tan\Psi = r d\phi/dr = 2f/(r\sin\theta)$$

for the parabola, and if we put $r = QP'$ and $\phi = 2\theta_i$ we find

$$\tan\Psi = \tan\theta_i$$

as expected.

The parametric representation of the CPC profile is easily obtained in Figure B2 if we take an origin for cartesian coordinates at the center of the exit aperture and z axis along the concentrator axis. We have from the figure

$$y = r\sin(\phi - \theta_i) - a' = \frac{2f\sin(\phi - \theta_i)}{1 - \cos\phi} - a'$$

$$= \frac{2a'(1 + \sin\theta_i)\sin(\phi - \theta_i)}{1 - \cos\phi} - a'$$

$$z = r\cos(\phi - \theta_i) = \frac{2a'(1 + \sin\theta_i)\cos(\phi - \theta_i)}{1 - \cos\phi}$$

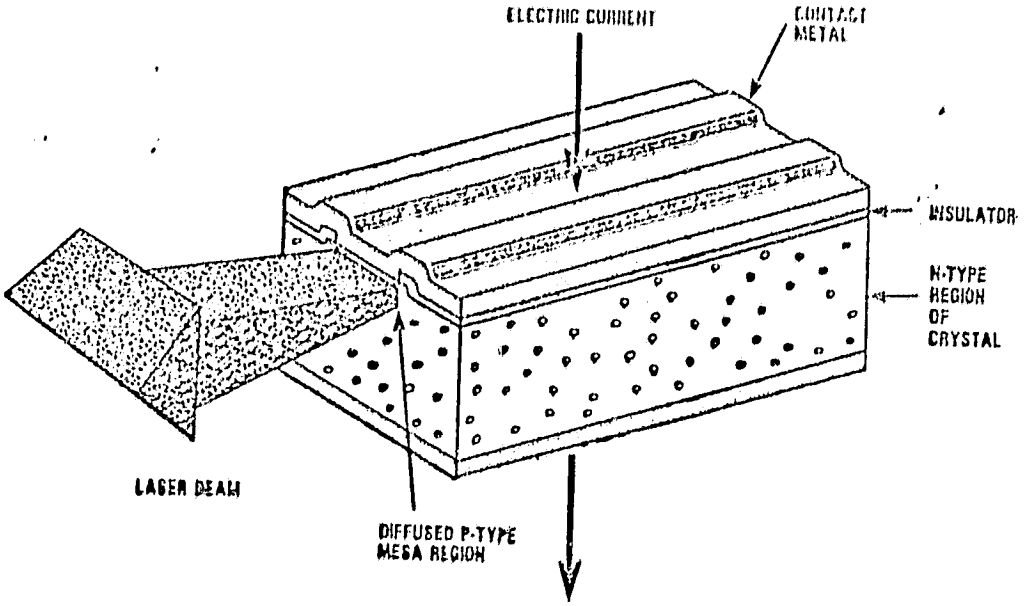

Fig.1

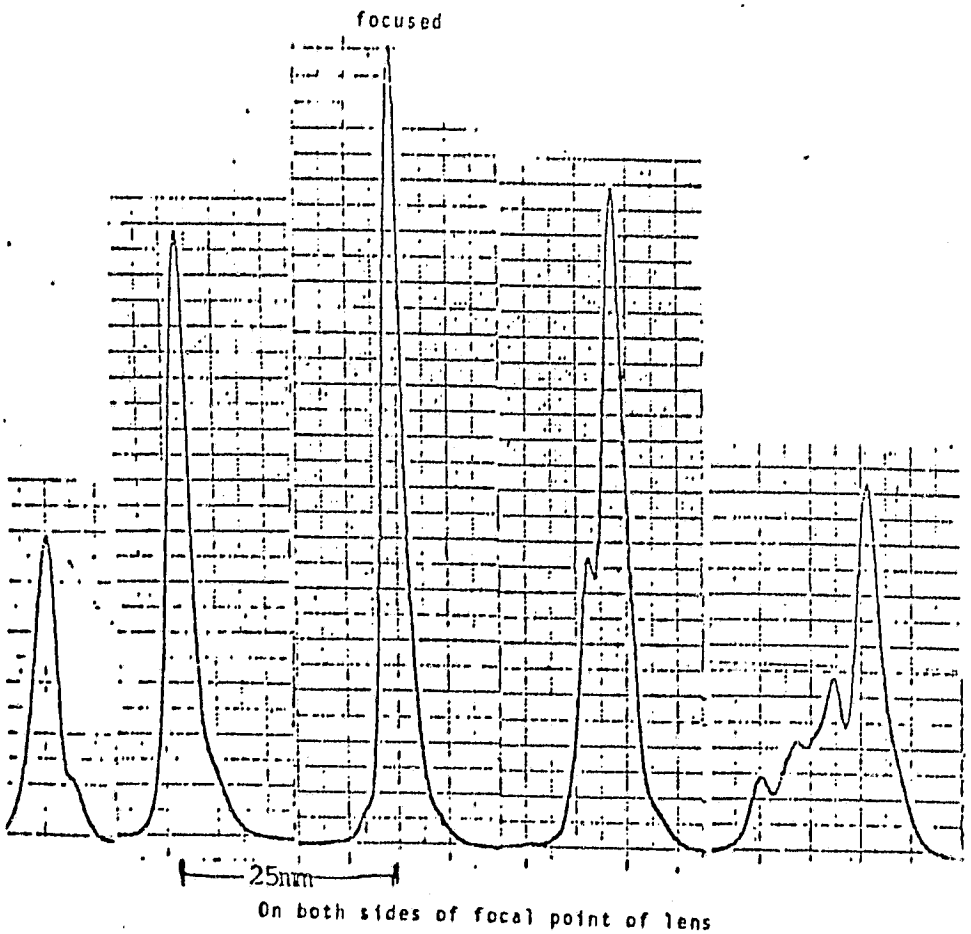

Fig.2

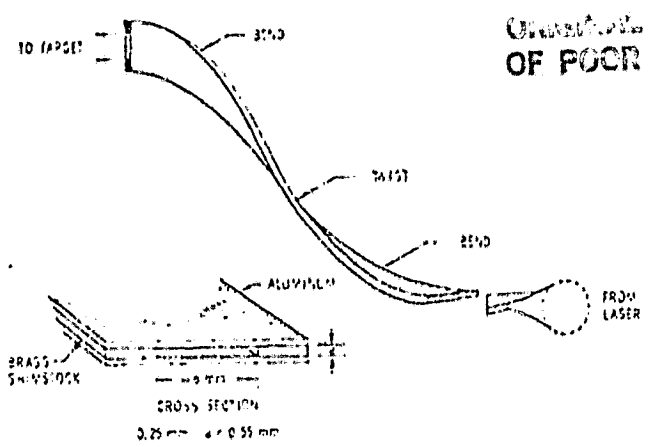

Fig. 3 Geometry of the FIT waveguide and details of its construction.

BEAM PROFILES REPORTED BY MANUFACTURER

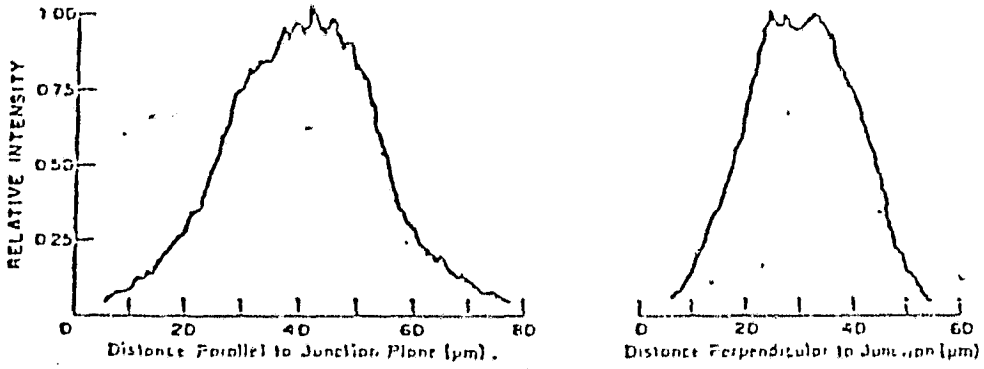

Mirror illumination pattern of a $Pb_{1-x}Sn_{x,y}Te$ 50-μm stripe laser running at 1 A, as obtained by scanning the magnified image of the laser end face with a small detector. For the scan parallel to the junction plane (y direction), the 53-μm width at e^{-2} percent power is in agreement with the width of the planar portion of the junction below the 50 μm contact stripe. The scan perpendicular to the junction (z direction) indicates illumination 42-μm wide.

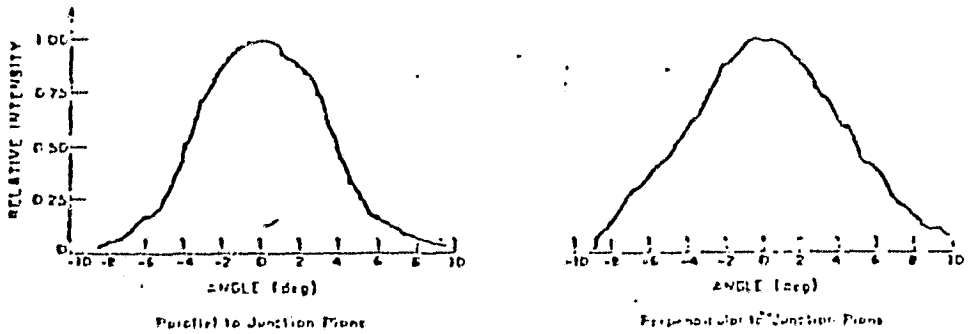

Far-field scan of a $Pb_{1-x}Sn_{x,y}Te$ 50-μm stripe laser operating 1 A pulsed at 4.2 K. The beam angle observed is consistent with a fundamental spatial mode emitted from the laser end face over a region of the size determined in the mirror illumination measurements

Fig.4 (Taken from Ref. 2)

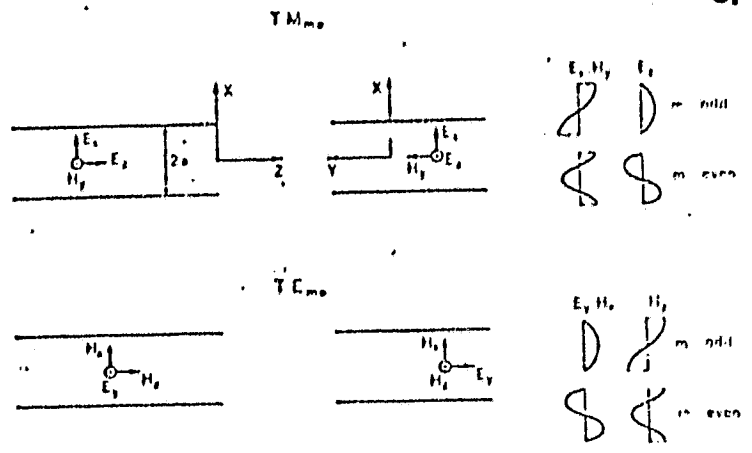

Fig 5 Field distributions for the TE and TM modes of two parallel metallic plates

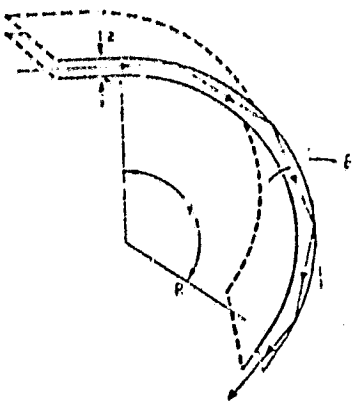

Fig 6 Geometry of bent waveguide, tracing the ray reflections for the conditions of a whispering gallery mode.

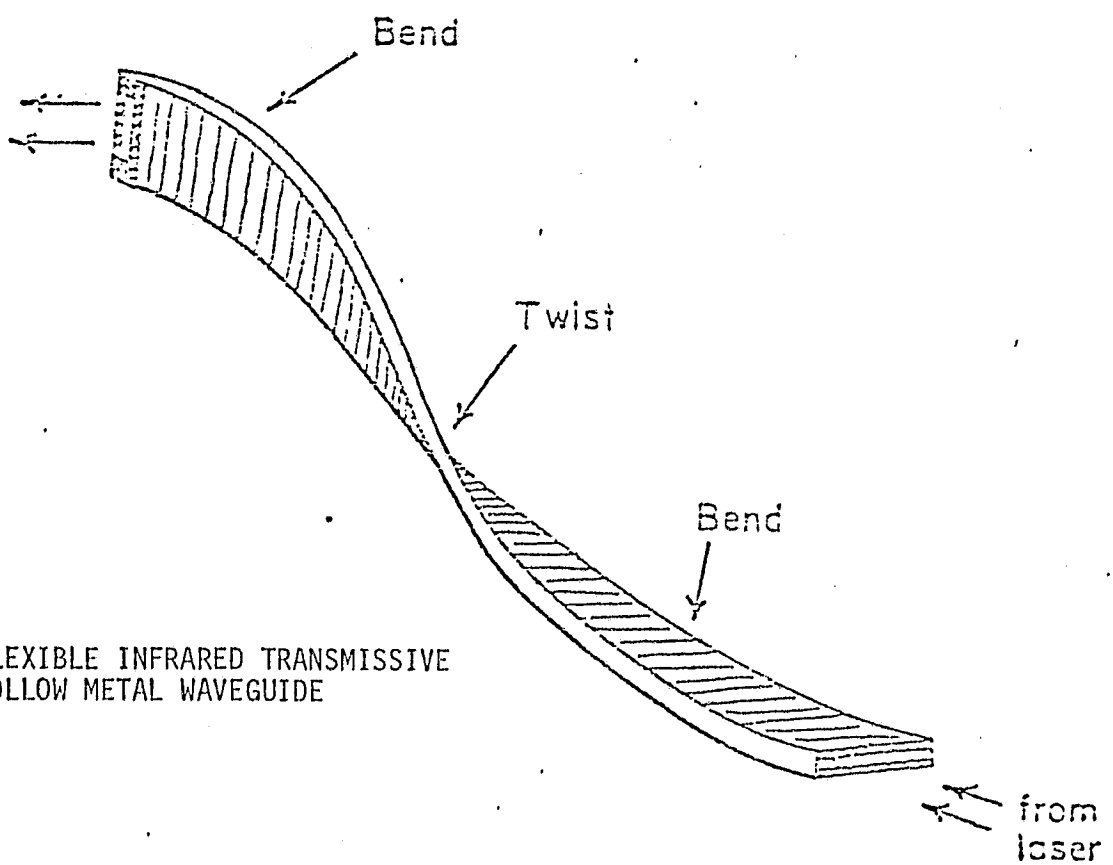

FLEXIBLE INFRARED TRANSMISSIVE
HOLLOW METAL WAVEGUIDE

Fig.7

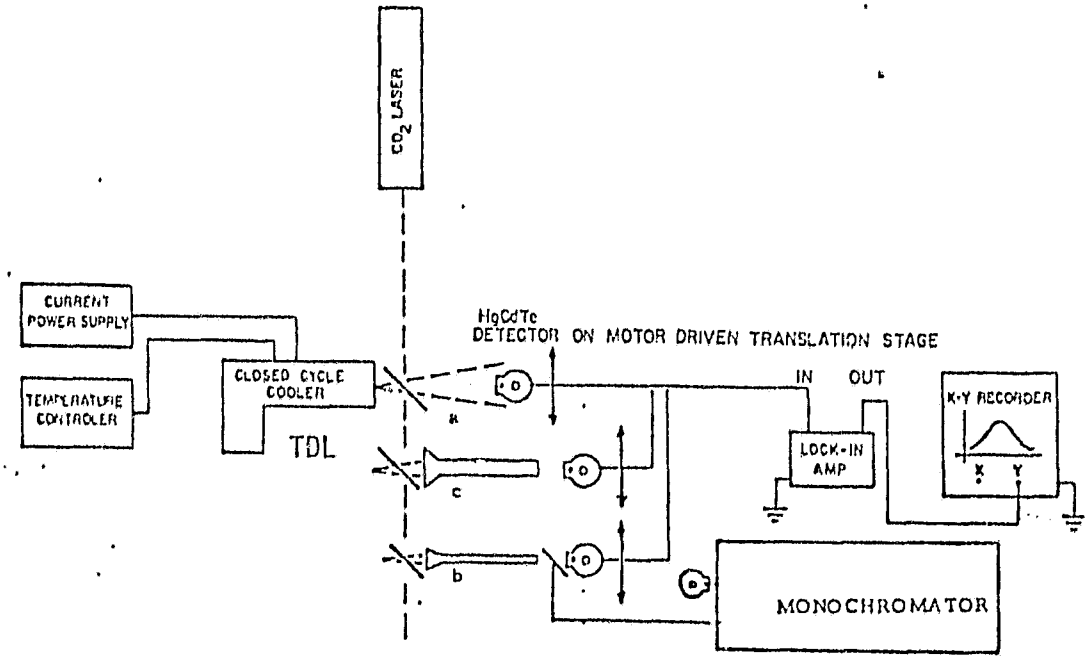

FIGURE 8 Experimental setup and pipe orientations (b, c).

ACTUAL PATTERNS OBSERVED
near cold head window

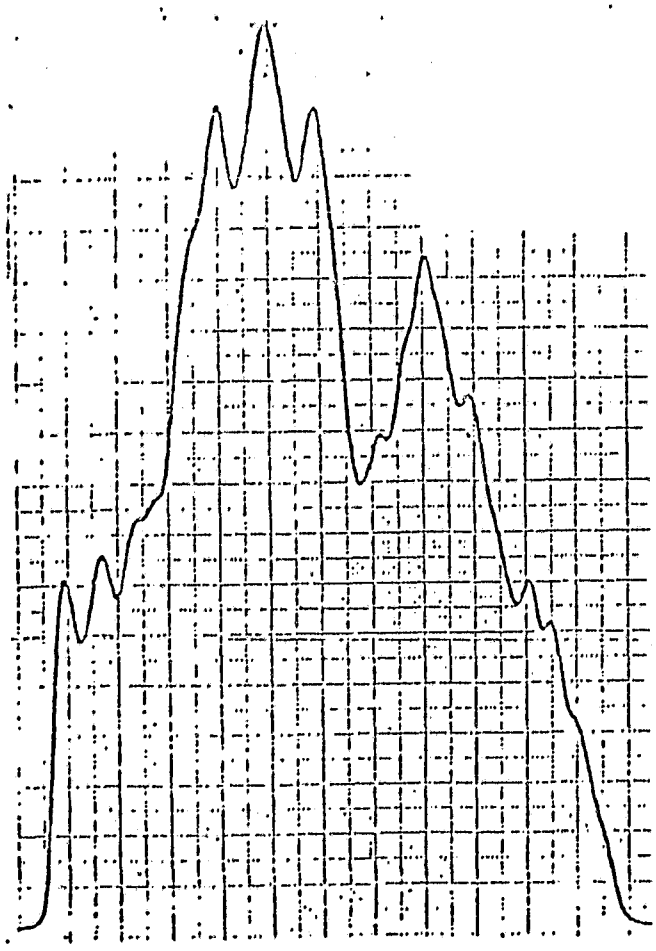

Fig.9

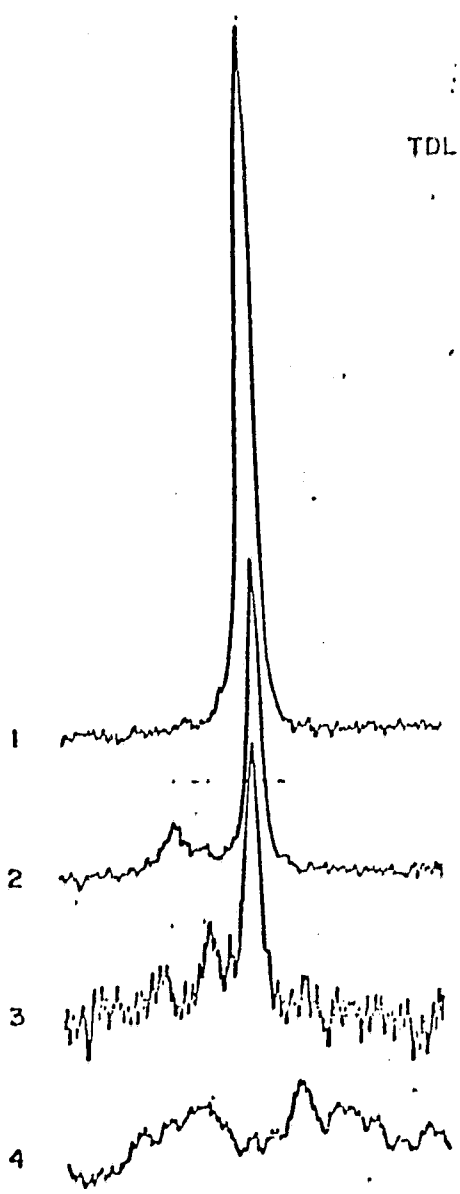

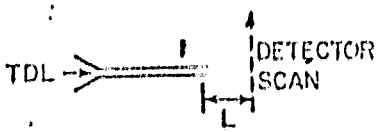

L =

1 - 1cm, 2 - 5", 3 - 9"
4 - NO PIPE, DETECTOR POSITION AS 3

Fig.10

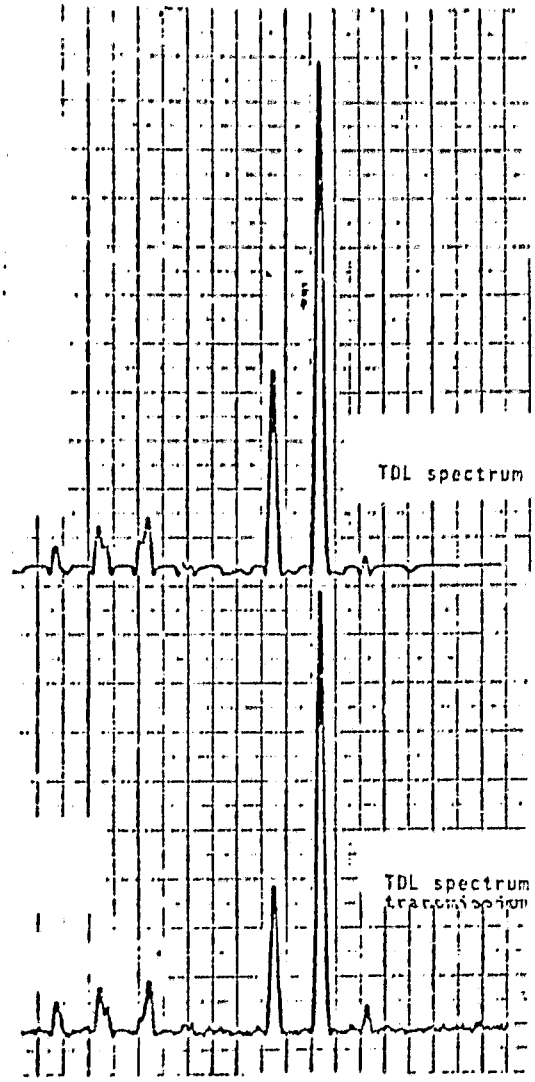

Fig.11

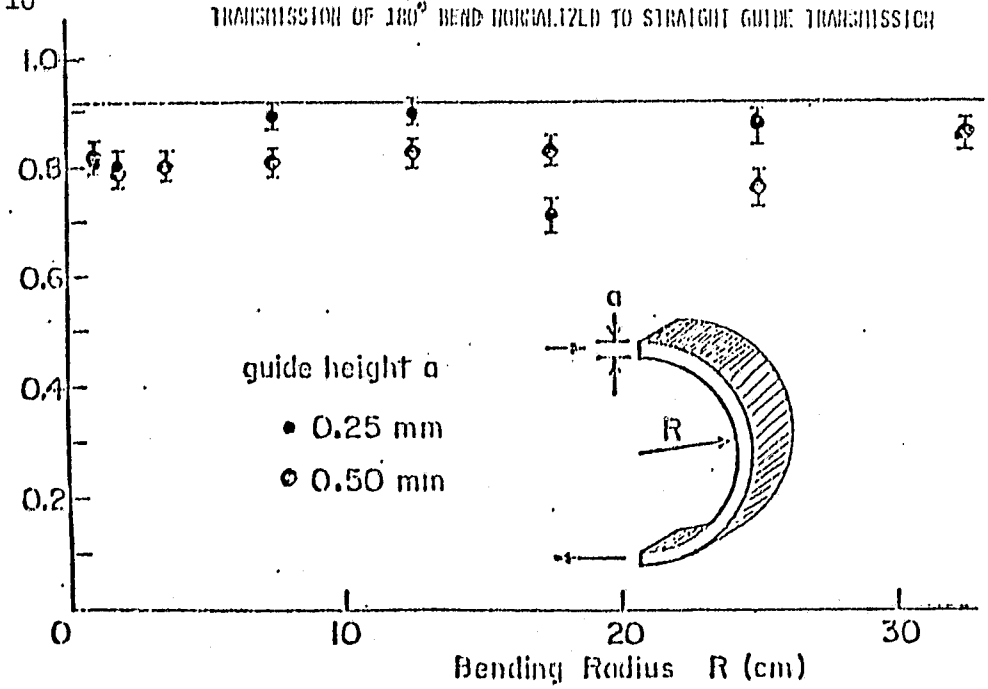

Fig.12 (Taken from Ref. 4)

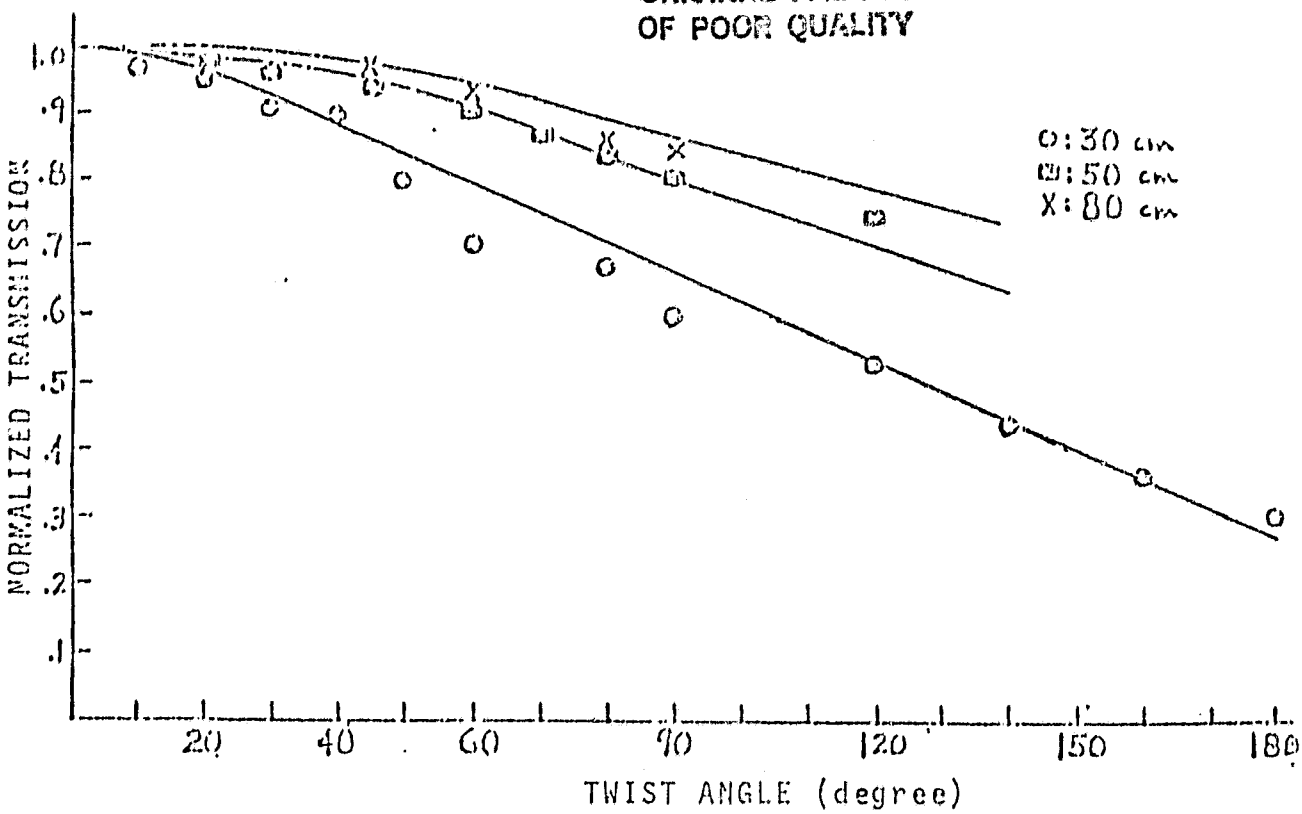

TRANSMISSION OF WAVEGUIDE TWIST

Figure 13 (Taken from Ref. 4)

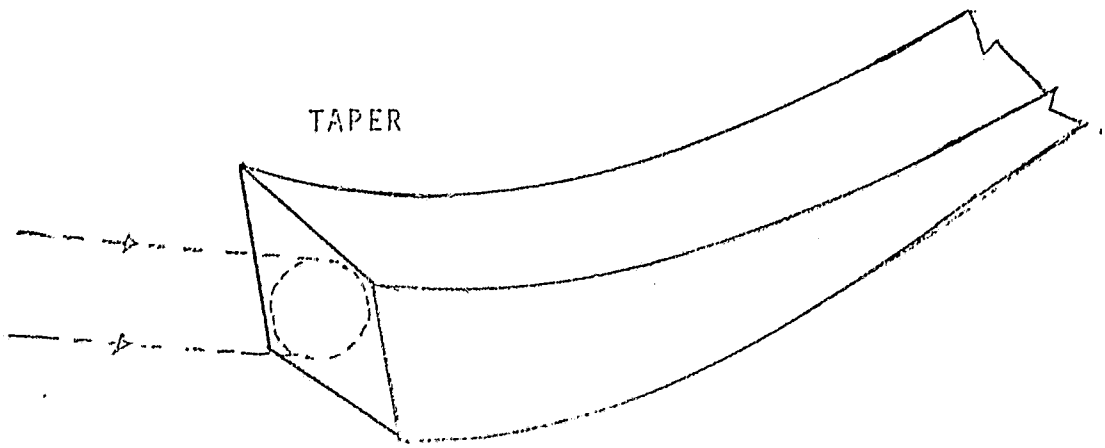

Figure 14

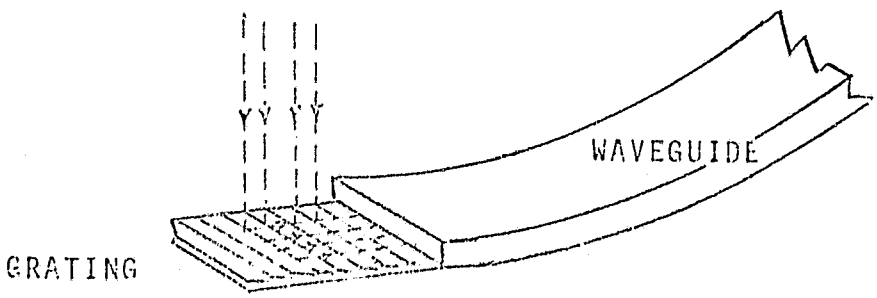

Figure 15

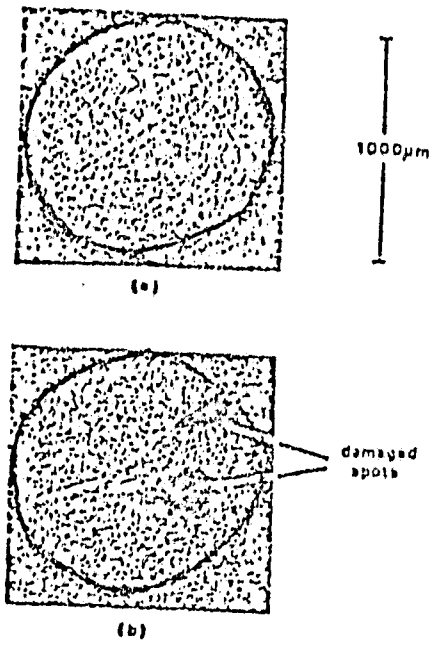

Fig.16 Microscopic photographs of power output end of a KRS-5 fiber: (a) before experiment, (b) after experiment. (Taken from Ref. 6)

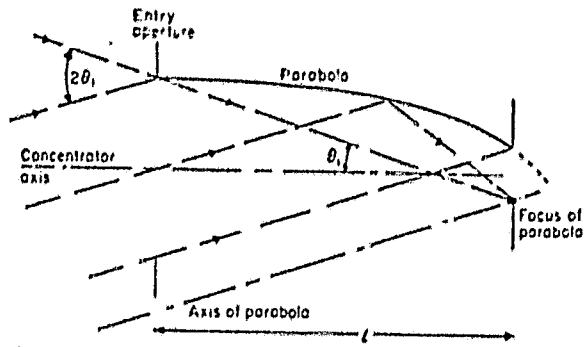

Fig.17 Construction of the CPC profile from the edge-ray principle.

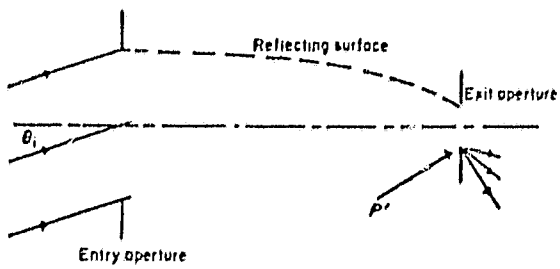

Fig.18 The edge-ray principle.

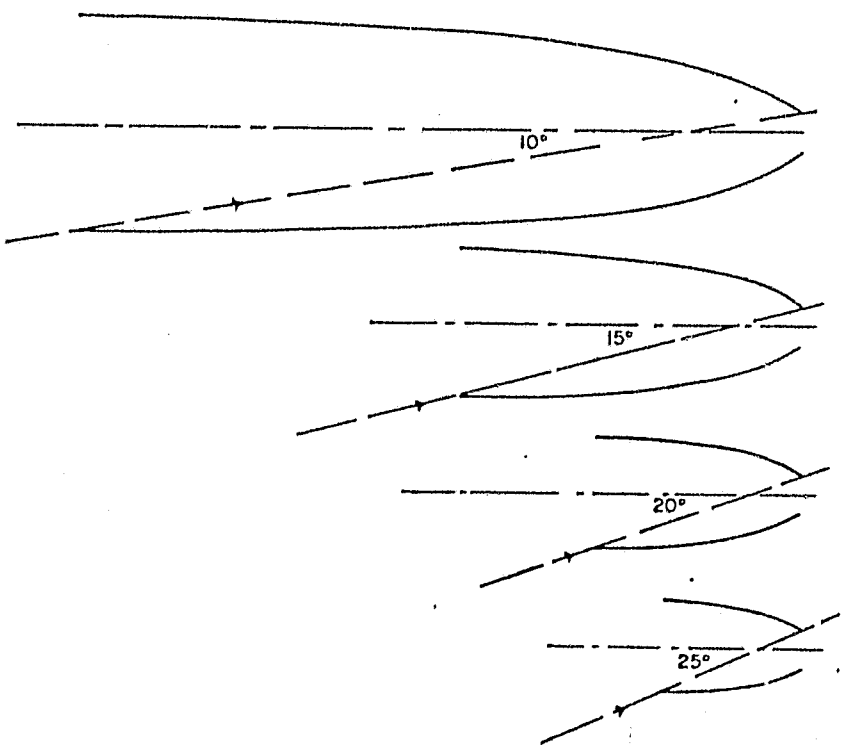

Fig 19 Some CPCs with different collecting angles. The drawings are to scale with the exit apertures all equal in diameter.

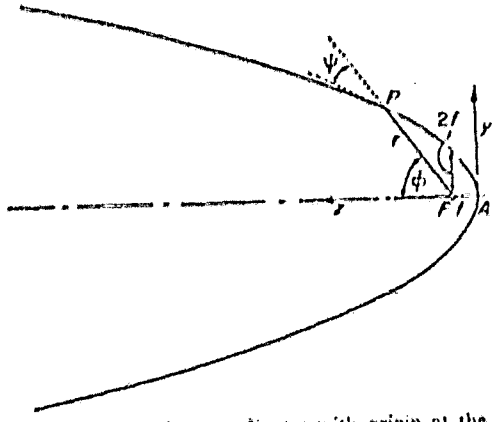

Fig.B-1 The parabola in polar coordinates with origin at the focus. $r = 2f(1 - \cos\phi) = f_1 \sin^2 \frac{1}{2}\phi$.

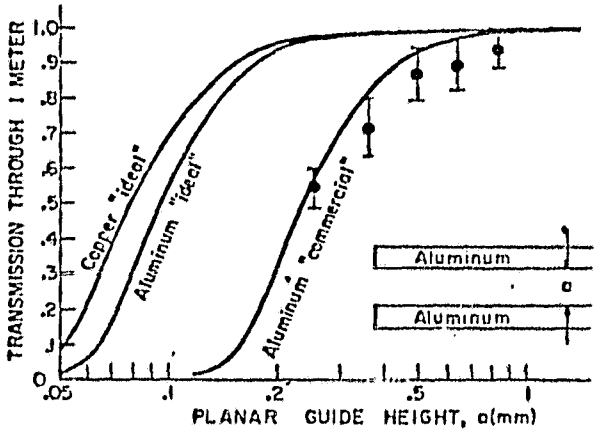

FIGA1. Transmission of a 1-m planar aluminum waveg a function of guide height. The waveguide geometry is s the inset.

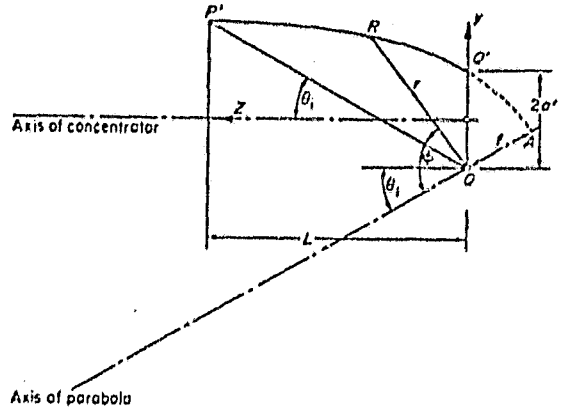

Fig. B.2 Design of the CPC.

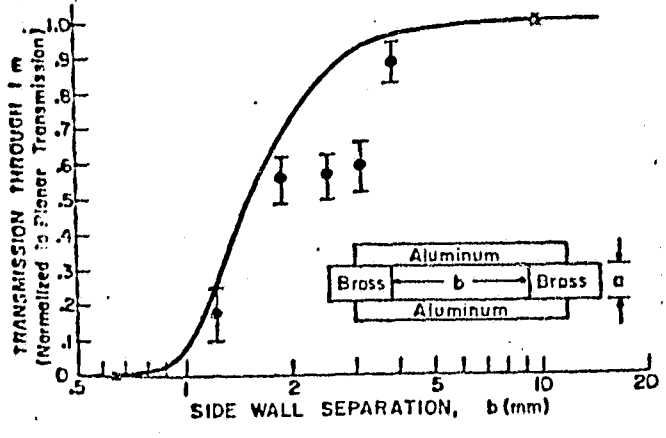

FIGA2. Transmission of a 1-m rectangular waveguide as a function of the guide width, normalized to the corresponding planar guide transmission.

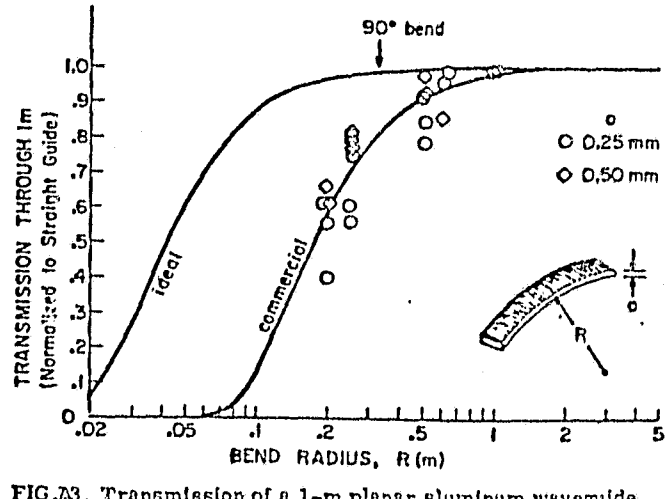

FIGA3. Transmission of a 1-m planar aluminum waveguide bent in a curve of radius R, normalized to the straight guide transmission.

(Figures A1, 2, 3 taken from Ref. 4)

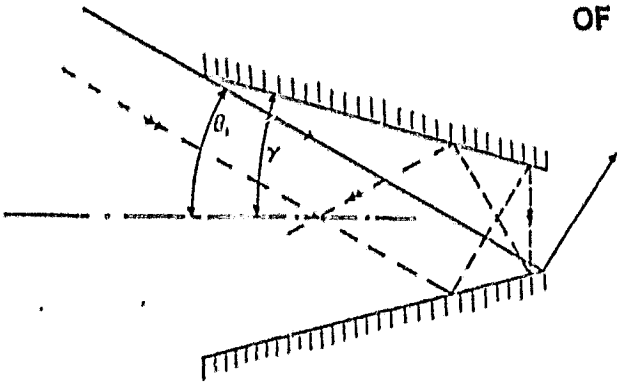

Fig. 20 The cone concentrator.

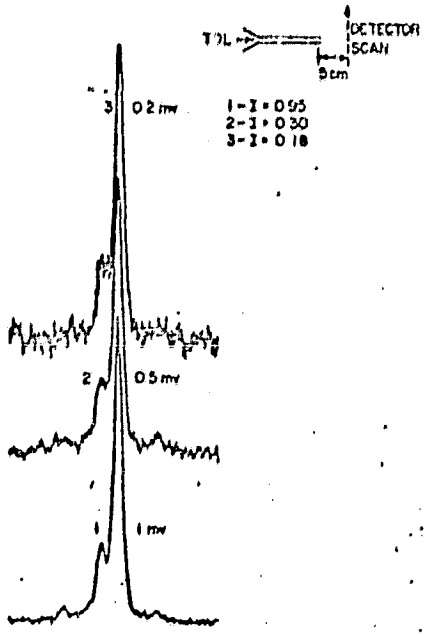

Fig.21 Pipe radiation patterns at different current drive.

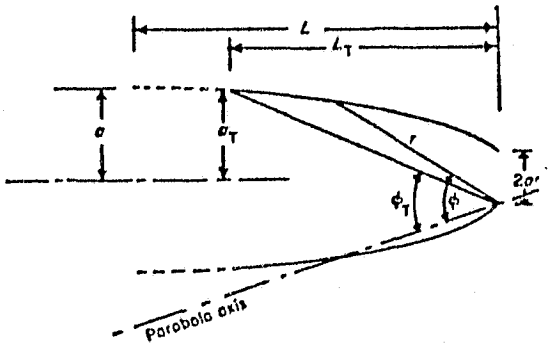

Fig. 22 The polar coordinates used in computing truncation effects.

REFERENCES

1. J. M. Hoell, C. N. Harward, and W. Lo, "High Resolution Atmospheric Spectroscopy Using a Diode Laser Heterodyne Spectrometer", Opt. Eng. 21, 320 (1982).

2. R. Ralston, I Melngailis, A. R. Calawa, and W. T. Lindley, "Stripe Geometry $Pb_{1-x}Sn_xTe$ Diode Lasers", IEEE J. Quantum Electron. 9, 350 (1973).
P. M. Asbeck, D. A. Cammack, and J. J. Daniele, "Non-Gaussian Fundamental Mode Patterns in Narrow Stripe Geometry Lasers", Appl. Phys. Lett. 33, 504 (1978).

3. C. Yu, "Beamshaping and Polarization Control Properties of Flexible Hollow Metallic Pipes in the Mid Infrared", Proc. IEEE 67, 965 (1979).

4. E. Garmire, T. McMahon, and M. Bass, "Flexible Infrared Transmissive Metal Waveguides", Appl. Phys. Lett. 29, 254 (1976).
E. Garmire, "Propagation of IR Light in Flexible Hollow Waveguides, Further Discussion", Appl. Opt. 15, 3037 (1976).
E .Garmire, T ,McMahon, and M. Bass, "Low loss Optical Transmission Through Bent Hollow Metal Waveguides", Appl. Phys, Lett. 31, 92 (1977).

5. N. K. Welker, and F. D. Bedard in AIP Conf. Proc. 44 on Future Trends in Superconducting Electronics, Charlottesville, VA (1978).

6. S .Sakuragi, M. Saito, Y. Kubo, H. Kotani, T. Morikawa, and J. Shimade, "KRS 5 Fibers Capable of Transmitting High-power CO_2 Laser Beam", Opt. Lett. 6, 629 (1981).

7. A. N. Paolantionio, "Military Fiber Optic Links: Can They Take the Heat? Microwaves 104 (January 1982).

8. W. T. Welford, and R. Winston, The Optics of Nonimaging Concentrators (Academic Press, New York, 1978) 1st Ed.